Bioconjugate Chemistry

Article

pubs.acs.org/bc

The Ionic Charge of Copper-64 Complexes Conjugated to an Engineered Antibody Affects Biodistribution

Jason L. J. Dearling,*[,†,‡] Brett M. Paterson,[§] Vamsidhar Akurathi,[†,‡] Soledad Betanzos-Lara,[†] S. Ted Treves,[†,‡] Stephan D. Voss,[†,‡] Jonathan M. White,[§] James S. Huston,[¶] Suzanne V. Smith,[#] Paul S. Donnelly,[§] and Alan B. Packard[†,‡]

[†]Division of Nuclear Medicine and Molecular Imaging, Department of Radiology, Boston Children's Hospital, Boston, Massachusetts 02115, United States

[‡]Harvard Medical School, Boston, Massachusetts 02115, United States

[§]School of Chemistry and Bio21 Molecular Science and Biotechnology Institute, The University of Melbourne, Parkville, VIC 3010, Australia

[¶]The Antibody Society & Huston BioConsulting LLC, Boston, Massachusetts 01908, United States

[#]Brookhaven National Laboratory, Upton, New York 11973, United States

Supporting Information

ABSTRACT: The development of biomolecules as imaging probes requires radiolabeling methods that do not significantly influence their biodistribution. Sarcophagine (Sar) chelators form extremely stable complexes with copper and are therefore a promising option for labeling proteins with ^{64}Cu. However, initial studies using the first-generation sarcophagine bifunctional chelator SarAr to label the engineered antibody fragment ch14.18-ΔC_H2 (MW 120 kDa) with ^{64}Cu showed high tracer retention in the kidneys, presumably because the high local positive charge on the Cu^{II}-SarAr moiety resulted in increased binding of the labeled protein to the negatively charged basal cells of the glomerulus. To test this hypothesis, ch14.18-ΔC_H2 was conjugated with a series of Sar derivatives of decreasing positive charge and three commonly used macrocyclic polyaza polycarboxylate (PAC) bifunctional chelators (BFC). The immunoconjugates were labeled with ^{64}Cu and injected into mice, and PET/CT images were obtained at 24 and 48 h postinjection (p.i.). At 48 h p.i., *ex vivo* biodistribution was assessed. In addition, to demonstrate the potential of metastasis detection using ^{64}Cu-labeled ch14.18-ΔC_H2, a preclinical imaging study of intrahepatic neuroblastoma tumors was performed. Reducing the positive charge on the Sar chelators decreased kidney uptake of Cu-labeled ch14.18-ΔC_H2 by more than 6-fold, from >45 to <6% ID/g, whereas the uptake in most other tissues, including liver, was relatively unchanged. However, despite this dramatic decrease, the renal uptake of the PAC BFCs was generally lower than that of the Sar derivatives, as was the liver uptake. Uptake of ^{64}Cu-labeled ch14.18-ΔC_H2 in neuroblastoma hepatic metastases was detected using PET.

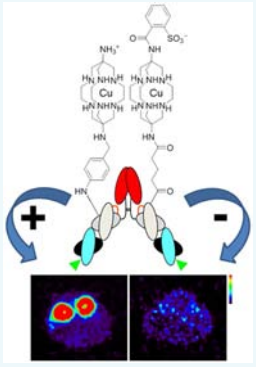

INTRODUCTION

Radiolabeled monoclonal antibodies are useful imaging agents because of their high specificity for the target antigen. When radiolabeled with a positron emitting radionuclide, they can provide quantitative, high-resolution data about the localization of a target antigen within the body. Antibody labeling with radioactive metals, such as ^{64}Cu ($t_{1/2}$ = 12.7 h, β^+ 17.9%, 653 keV), requires the use of a bifunctional chelator (BFC) to attach the radioactive metal to the protein, ideally without adversely affecting the pharmacokinetics of the antibody. The resulting metal-BFC complex must be stable *in vivo* for the imaging data to accurately reflect the distribution of the antibody. While DOTA (1,4,7,10-tetraazacyclododecane tetraacetic acid) has often been used as a BFC, despite the fact that the kinetic instability of its copper complex[1] can lead to loss of the ^{64}Cu from the radioimmunoconjugate (RIC), there is considerable interest in developing BFCs that form ^{64}Cu complexes that are more kinetically stable *in vivo*. One example is the sarcophagine-based BFCs, which have shown considerable promise in this application because of the very high stability of their copper complexes.[2]

Although PET imaging with ^{64}Cu-labeled antibodies offers high specificity for the characterization of tumors, it is limited by the slow clearance of the RICs from normal tissues, including the blood. Fortunately, the pharmacokinetics of antibodies can be improved through protein engineering,[3] including reducing the size of the construct. For example, removing the C_H2 domain from the whole IgG antibody (MW 150 kDa) reduces the molecular weight of the protein to approximately 120 kDa (Figure 1). This results in more rapid clearance from nontarget tissues and thus a shorter delay between tracer injection and imaging while also reducing the radiation exposure of nontarget tissue. The trade off is that the smaller molecular weight also decreases absolute tumor uptake

Received: January 22, 2015
Revised: February 25, 2015
Published: February 26, 2015

DOI: 10.1021/acs.bioconjchem.5b00049
Bioconjugate Chem. 2015, 26, 707−717

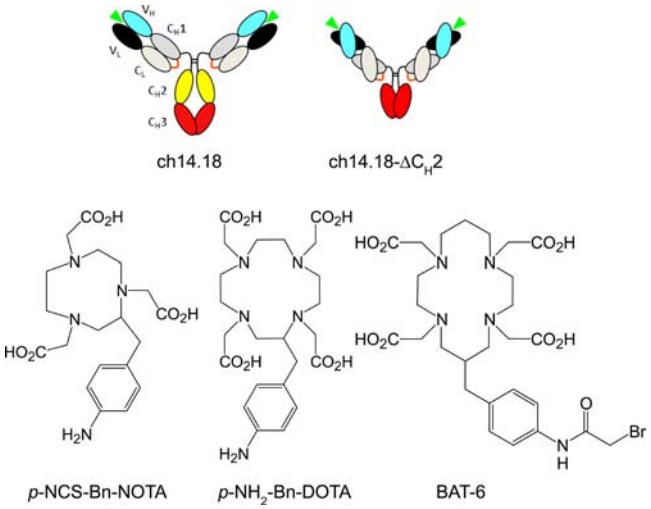

Figure 1. (Top) Structures of the whole antibody, ch14.18, and the engineered form used in this study, ch14.18-ΔC_H2 (green arrows show the antigen-binding regions). (Bottom) Structures of the three macrocyclic polyaza polycarbolxylate bifunctional chelators: NOTA, DOTA, and TETA (left to right).

because the time during which the protein can accumulate in the tumor tissue is reduced.[4] The goal, therefore, is to find the optimal balance between tumor uptake and clearance from nontarget tissues.

The ΔC_H2 immunoprotein format[5] was examined in several previous studies, including those aimed at developing imaging probes. For example, Slavin-Chiorini et al. and Chinn et al. reported shorter blood half-lives for radioiodinated and ^{111}In-labeled HuCC49.ΔC_H2 proteins compared with that of intact antibodies.[6,7] Mueller et al.[8] reported similar findings for the radioiodinated anti-GD2 antibody ch14.18-ΔC_H2, suggesting that it was a promising format for further study as a radiolabeled imaging agent.

Neuroblastoma, the most common extracranial solid tumor in children, presents with large clinical heterogeneity. Early stage disease (i.e., I or II) typically responds well to therapy, whereas advanced-stage disease (i.e., III and IV) is typically more resistant. As with many malignancies, improved detection and characterization of neuroblastoma is critical to designing patient-specific therapeutic regimes. In current practice, patients with neuroblastoma are typically imaged with various radiopharmaceuticals including [^{18}F]FDG, [^{123}I]mIBG, and ^{99m}Tc-MDP.[9,10] The evaluation of [^{18}F]FDG imaging in children following radiation therapy, chemotherapy, and surgery is complicated by the effects of these treatments. Iodine-labeled mIBG is very specific, but the value of post-therapy scans is controversial because uptake can persist long after effective treatment, producing a false positive result.[11,12] Technetium-99m-MDP is considered to be useful in initial staging, especially for bone metastases, but not in later restaging studies or in assessing response to therapy, again because of the effects of therapy.[9] Consequently, there remains a clinical need for a more specific imaging probe for the detection and monitoring of neuroblastoma.

GD2 is a disialoganglioside that is expressed at high levels on the surface of neuroblastoma tumor cells but is not found in normal tissue,[13,14] making it a promising target for antibody-based *ex vivo* cytochemical identification,[15,16] imaging,[17−19] and therapy[20] of neuroblastoma. Clinical studies, including those by Reuland et al.[18] and Yeh et al.,[21] have described the advantages of anti-GD2 radioimmunoimaging over ^{123}I-mIBG imaging, including its ability to provide early information about response to therapy and disease progression. Intact radiolabeled anti-GD2 antibodies, however, are suboptimal as imaging agents because the clearance half-life from nontarget tissue is up to 3 days.

In previous work, we described the use of SarAr for radiolabeling the anti-GD2 antibody ch14.18 with ^{64}Cu and compared the biodistribution of ^{64}Cu-SarAr-ch14.18 to that of ch14.18 labeled with ^{64}Cu using other BFCs.[22] However, the biological half-life of this radioimmunoconjugate is somewhat longer than is desirable for an imaging agent. In contrast, ^{64}Cu-labeling of ch14.18-ΔC_H2 using SarAr as the BFC could produce a neuroblastoma imaging agent with high specificity, improved pharmacokinetics, and high *in vivo* retention of the ^{64}Cu label. Unfortunately, initial studies of ^{64}Cu-SarAr-ch14.18-ΔC_H2 showed very high renal uptake, which we hypothesized was due to the high net positive charge of the Cu-SarAr moiety. To test this hypothesis, we have prepared a series of Sar-based chelators with lower net positive charges than that of SarAr (Figure 2) and compared the biodistribution of ch14.18-ΔC_H2 labeled with ^{64}Cu using these BFCs with that of several commonly used polyaza polycarboxylate BFCs (DOTA, NOTA, and TETA; Figure 1). On the basis of the results of this screening study, we evaluated the most promising of the radioimmunoconjugates in a mouse model of metastatic neuroblastoma.

RESULTS

Synthesis. The complex $[Cu(NH_3)(CO_2CH_3)sar](CF_3SO_3)_3$ was synthesized from $[Cu(NH_2)(CO_2H)sar]^{2+}$. Copper ion coordination was used to protect the secondary amine groups of $[Cu(NH_3)(CO_2CH_3)sar](CF_3SO_3)_3$ for selective acylation of the primary amine with 2-sulfobenzoic anhydride (Figure 2, top). To simplify isolation, the carboxylic acid was esterified to the methyl ester so that the resulting sulfonated Cu^{II} complex had a positive charge, allowing purification by cation exchange chromatography. Following purification, the ester was hydrolyzed by treatment with strong acid and the product, $Cu(SO_3)(CO_2)sar$, was isolated by neutralization with Dowex 1 × 8 anion exchange resin (acetate form). Crystals of $Cu(SO_3)(CO_2)sar{\cdot}9(H_2O)$ were generated by vapor diffusion of acetone into a solution of the complex in water and analyzed by X-ray crystallography (Figure 3; see also Supporting Information Table S1). The structural analysis shows the complex to be a neutral zwitterion with the positive charge of the Cu^{II} offset by the deprotonated sulfonate and carboxylate groups. The coordination environment about the Cu^{II}, similar to other examples of Cu^{II} complexes with N6-sarcophagine ligands, reflects a combination of trigonal distortions imposed by the ligand and tetragonal distortions due to the Jahn−Teller effect of the d^9 Cu^{II}. The Cu−N bond lengths of the distorted octahedral $Cu(SO_3)(CO_2)sar$ complex range from 2.244(3) to 2.107(4) Å, and numerous hydrogen bonds are evident with solvent water molecules as well as between neighboring complexes within the lattice. The aliphatic carboxylate functional group extends away from the macrobicyclic cage, which is present in the *lel*$_3$ conformation, where the C−C bonds of the five-membered chelate rings are parallel to the pseudo-C_3 axis.

The metal ion was removed from $Cu(SO_3)(CO_2)sar$ by reducing the Cu^{II} with $NaBH_4$ and Pd/C followed by

DOI: 10.1021/acs.bioconjchem.5b00049
Bioconjugate Chem. 2015, 26, 707−717

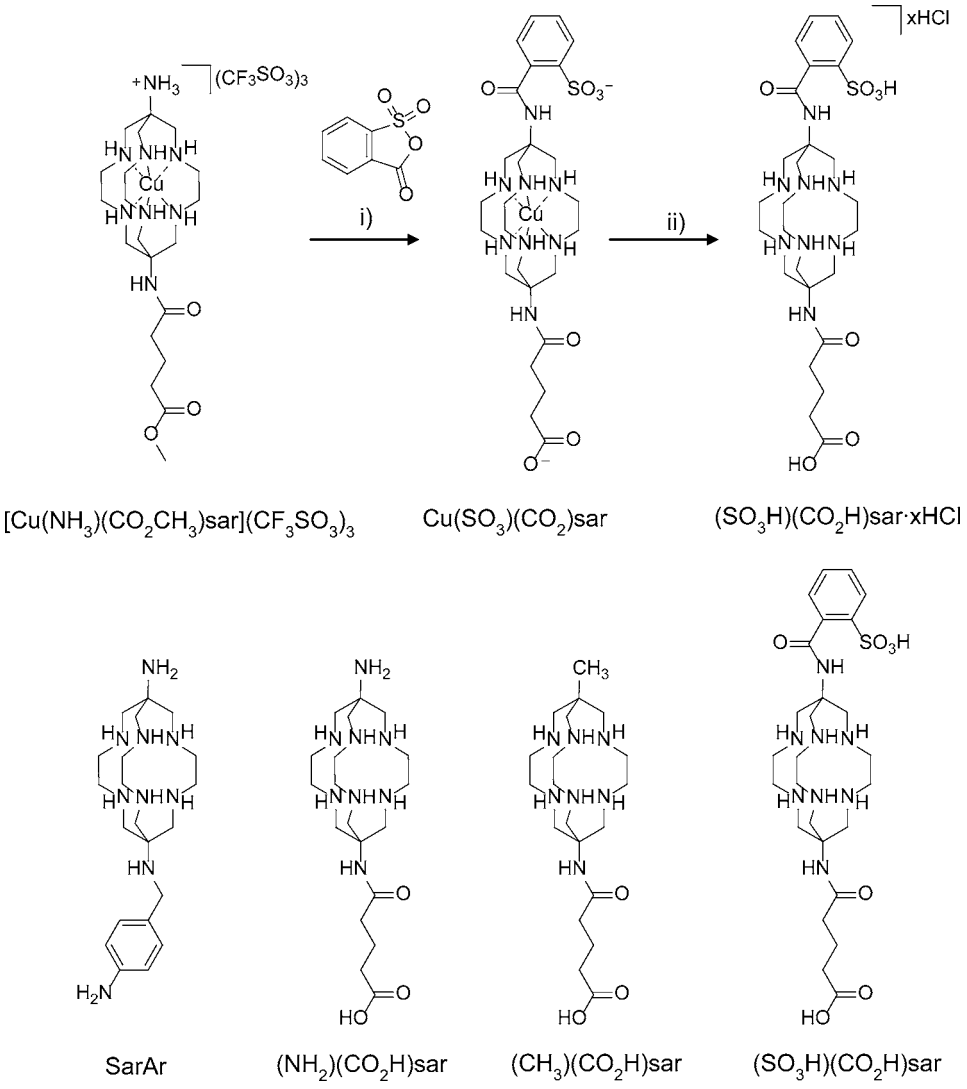

Figure 2. (Top) Synthetic scheme for $(SO_3H)(CO_2H)$sar: (i) DIPEA, DMA, H^+/H_2O; (ii) NaOH (0.2 M), $NaBH_4$, Pd/C, HCl. (Bottom) Structures of the Sar-based bifunctional chelators used in this study.

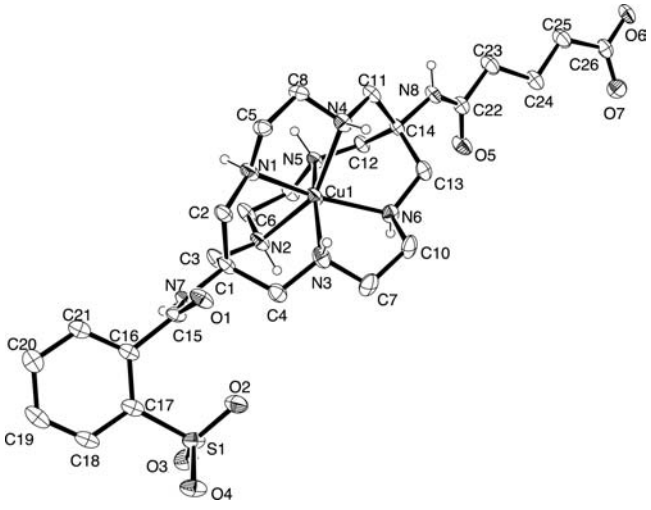

Figure 3. A thermal ellipsoid plot for $Cu(SO_3)(CO_2)$sar·$9(H_2O)$. Hydrogen atoms bonded to carbon and solvent have been omitted for clarity.

purification by cation exchange chromatography to give the free ligand, $(SO_3H)(CO_2H)$sar.

Conjugation, Antigen Binding, and Radiolabeling. Examples of the ELISA results are presented in Figure 4. The study demonstrated that all of the immunoconjugates retained antigen binding following conjugation.

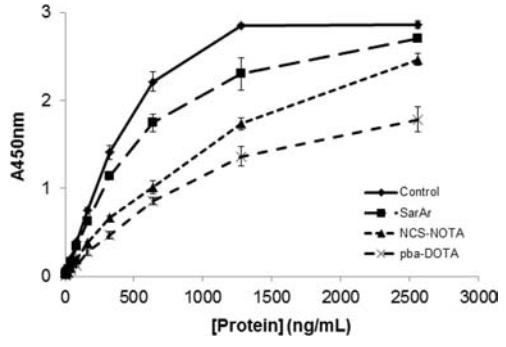

Figure 4. Example ELISA data for the ch14.18-ΔC_H2 antibody and three immunoconjugates. The data confirmed that all of the immunoconjugates retained antigen binding following conjugation.

DOI: 10.1021/acs.bioconjchem.5b00049
Bioconjugate Chem. 2015, 26, 707−717

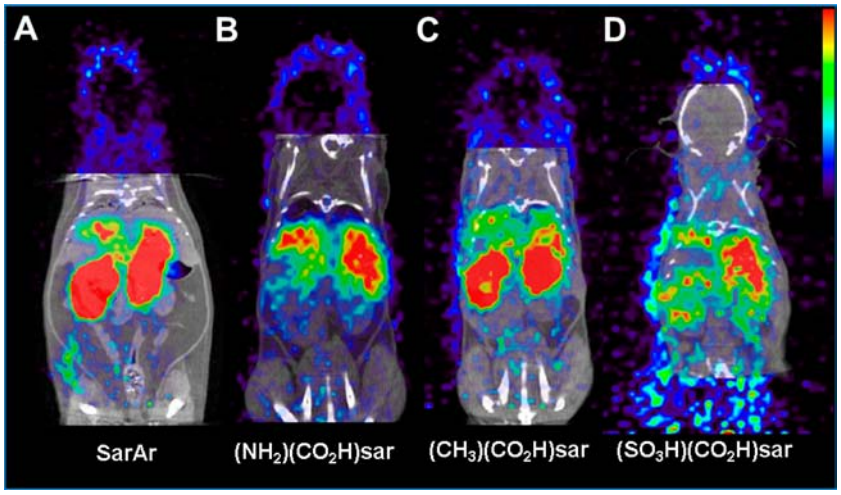

Figure 5. Coronal small animal PET/CT images of mice injected with ch14.18-ΔC_H2 labeled with ^{64}Cu via SarAr (A), $(NH_2)(CO_2H)$sar (B), $(CH_3)(CO_2H)$sar (C), and $(SO_3H)(CO_2H)$sar (D) at 48 h postinjection. PET data is in color scale; CT data is in gray scale.

The number of available chelators attached to each antibody fragment was found to range from 0.18 ± 0.008 to 2.0 ± 0.4 (means of three separate determinations ± ESD). The immunoconjugates were labeled to specific activities of 0.073−0.15 MBq (1.98−4.03 μCi) per microgram of protein.

Imaging and Biodistribution. Examples of images from data collected at 48 h p.i. for the Sar-based chelators are presented in Figure 5. For ^{64}Cu-SarAr-ch14.18-ΔC_H2 (Figure 5A), the kidney dominates the image, whereas kidney uptake was lower for the ^{64}Cu-$(NH_2)(CO_2)$sar-ch14.18-ΔC_H2 study (Figure 5B). For ^{64}Cu-$(CH_3)(CO_2)$sar-ch14.18-ΔC_H2 (Figure 5C), kidney uptake was lower than that of ^{64}Cu-SarAr-ch14.18-ΔC_H2, and kidney uptake of ^{64}Cu-$(SO_3)(CO_2)$sar-ch14.18-ΔC_H2 (Figure 5D) was further decreased, with some liver uptake evident.

The results of the analysis of the PET data are presented in Figure 6. Generally, normal tissue uptake of the RICs incorporating Sar-based BFCs was higher than that of the PACs, particularly in the liver and kidney. Liver uptake of the Sar-based BFCs was within the range 10−20% ID/g. Within the Sar-based BFCs, the greatest and most significant change was in kidney uptake.

Interestingly, changing the apical primary amine, which is likely to be protonated at physiological pH *in vivo*, of the sarcophagine cage (SarAr) to a methyl group ($(CH_3)(CO_2H)$-sar) led to a decrease in kidney uptake, and a further decrease was achieved when the apical group was an aromatic sulfonate. Among the PAC BFCs, there is an overall pattern of low uptake in most tissues as well as rapid clearance. The greatest difference was seen in the liver data, i.e., using DOTA as the BFC resulted in high hepatic uptake relative to that with the other two PAC BFCs. Kidney uptake for the PAC BFCs is comparable to that of the lowest of the Sar-based chelators.

The results of the 48 h biodistribution study are summarized in Table 1. Aside from the high kidney uptake of SarAr- and $(CH_3)(CO_2)$sar-labeled protein (47 and 28% ID/g, respectively), the tissue distributions of ch14.18-ΔC_H2 labeled via these BFCs are similar to those of the PAC BFCs. At 48 h p.i., the blood concentration of the ^{64}Cu-DOTA-protein (2.1% ID/g) was significantly higher than that of the other RICs except for that incorporating $(SO_3)(CO_2)$sar (1.7% ID/g). Uptake of the ^{64}Cu-labeled proteins using Sar-based BFCs in the heart was generally higher than that seen with the PAC-labeled

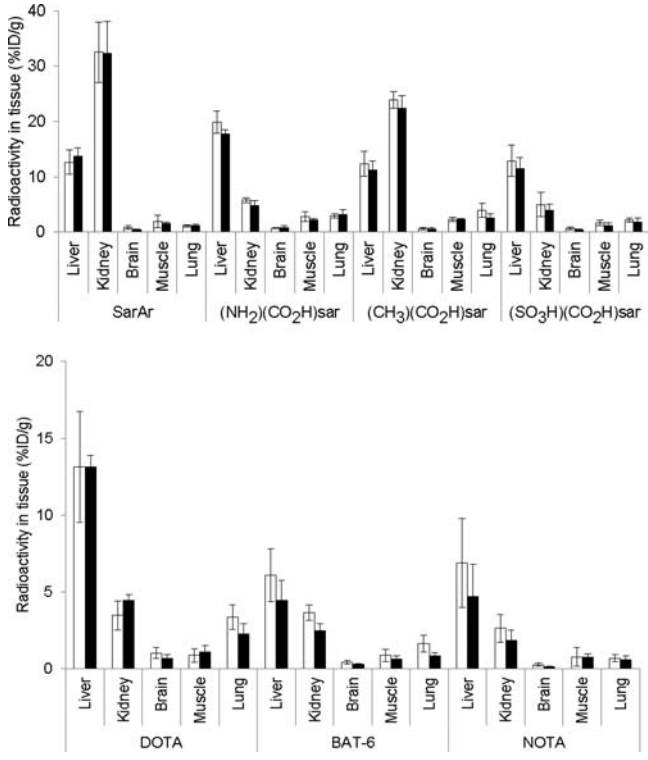

Figure 6. Bar graphs of small animal PET data for the BFCs incorporating the sarcophagine chelators (top) and the polyaminocarboxylate chelators (bottom). Data presented are for 24 (white) and 48 h (black) postinjection. Note the different *y*-axis scales.

proteins. In the lung, the $(SO_3)(CO_2)$sar and DOTA RIC concentrations were both relatively high, possibly because of their higher blood concentration. The liver concentrations of the BAT-6- and NOTA-conjugated proteins were lower than those of the other BFCs. Overall, gut uptake was low, with similar numbers for all the BFCs, with DOTA being the highest uptake (possibly because of its higher liver concentration) and NOTA and BAT-6 being the lowest. Brain uptake was low (as expected for a large protein), with DOTA showing the highest uptake (0.34% ID/g).

DOI: 10.1021/acs.bioconjchem.5b00049
Bioconjugate Chem. 2015, 26, 707−717

Table 1. Summarizing 48 h *Ex Vivo* Biodistribution Data and the Results of Statistical Analysis[a]

	SarAr	$(NH_2)(CO_2H)$sar	$(CH_3)(CO_2H)$sar	$(SO_3H)(CO_2H)$sar	*p*-NH_2-Bn-DOTA	BAT-6	*p*-NCS-Bn-NOTA
tissue	1	2	3	4	5	6	7
blood	0.34 (0.04)	0.67 (0.13)	0.68 (0.07)	1.66 (0.22)	2.12 (1.20)	0.66 (0.11)	0.16 (0.04)
	5	*5*	*5*	*7*	*1, 2, 3, 6, 7*	*5*	*4, 5*
heart	2.89 (0.58)	2.39 (0.82)	3.42 (0.70)	1.98 (0.50)	1.68 (0.21)	1.01 (0.15)	0.61 (0.15)
	6, 7	*7*	*5, 6, 7*		*3*	*1, 2, 3*	*1, 2, 3*
lung	1.63 (0.25)	1.70 (0.06)	2.31 (0.32)	1.95 (0.49)	2.99 (0.42)	1.41 (0.11)	0.57 (0.18)
	5, 7	*5, 7*	*6, 7*	*5, 7*	*1, 2, 4, 6, 7*	*3, 5*	*1, 2, 3, 4, 5*
liver	13.8 (1.8)	15.7 (1.0)	9.3 (1.5)	10.2 (3.3)	13.6 (2.1)	3.6 (1.5)	4.0 (1.1)
	6, 7	*3, 6, 7*	*2, 6*	*6, 7*	*6, 7*	*1, 2, 3, 4, 5*	*1, 2, 4, 5*
spleen	8.79 (4.44)	9.33 (3.38)	7.61 (2.06)	6.18 (3.03)	6.08 (2.53)	1.64 (0.38)	1.60 (0.10)
kidney	46.9 (6.5)	5.48 (0.40)	28.4 (4.8)	6.64 (2.08)	4.22 (0.97)	2.40 (0.39)	1.88 (0.42)
	2, 3, 4, 5, 6, 7	*1, 3*	*1, 2, 4, 5, 6, 7*	*1, 3*	*1, 3*	*1, 3*	*1, 3*
gut	1.99 (0.34)	1.50 (0.08)	1.92 (0.37)	2.02 (1.69)	2.42 (0.21)	1.00 (0.31)	0.57 (0.04)
					7		*5*
brain	0.10 (0.05)	0.09 (0.02)	0.11 (0.02)	0.11 (0.01)	0.34 (0.09)	0.11 (0.03)	0.06 (0.02)
	5	*5*	*5*	*5*	*1, 2, 3, 4, 6, 7*	*5*	*5*
muscle	0.62 (0.13)	1.02 (0.18)	0.87 (0.24)	0.57 (0.12)	0.42 (0.13)	0.24 (0.05)	0.12 (0.03)
	2, 6, 7	*1, 4, 5, 6, 7*	*5, 6, 7*	*2, 7*	*2, 3*	*1, 2, 3*	*1, 2, 3, 4*
bone	2.33 (0.51)	1.02 (0.18)	1.92 (0.15)	1.53 (0.48)	1.58 (0.41)	1.23 (0.89)	0.65 (0.21)
	7	*4, 5, 6, 7*		*2*	*2*	*2*	*1, 2*
n	5	3	3	3	4	3	3

[a]Biodistribution data is given as % ID/g mean, with SD in parentheses. Statistical analysis was performed by ANOVA. Numbers in italic font indicate significant difference ($p < 0.05$, Bonferroni correction) compared with the indicated chelate.

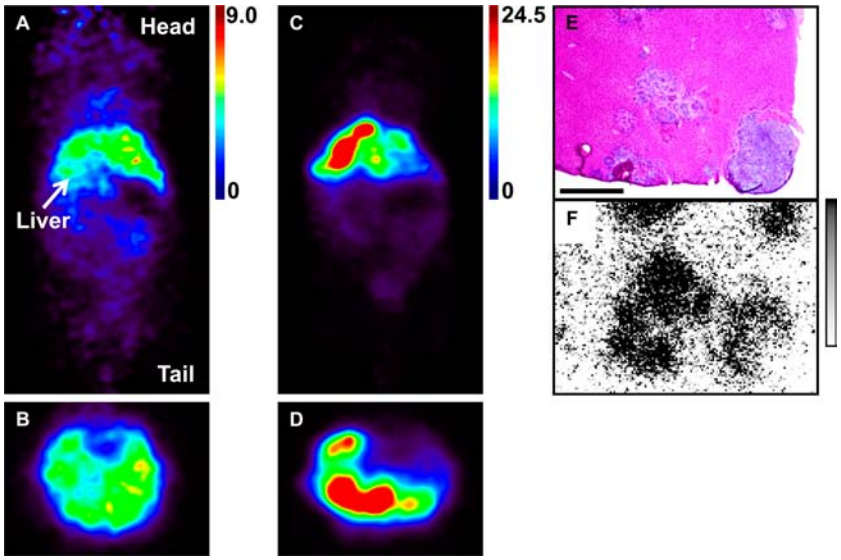

Figure 7. Uptake of ^{64}Cu-NOTA-ch14.18-ΔC_H2 in a model of neuroblastoma metastases. Typical small animal PET images of distribution of the imaging agent in mice at 4 h p.i. are shown. Images of mice without (A, B) and with metastases (C, D; coronal top and transaxial bottom) are presented for comparison, and scales for each set of images are shown at the right (% ID/g). (E) H&E stain of tissue section (1 mm scale bar bottom left) and (F) autoradiography (scale at right) show small tumors (purple) throughout the liver (pink) with radionuclide concentrated in tumor.

Metastatic Model of Neuroblastoma. Imaging of three mice bearing intrahepatic metastases revealed high multifocal uptake of ^{64}Cu-NOTA-ch14.18-ΔC_H2 in the liver metastases throughout the imaging time course (1 to 48 h).

Typical images are shown in Figure 7. Histological analysis of the H&E stained tissue sections (Figure 7E) revealed small tumors with a diameter of approximately 1 mm throughout the liver with some concentration toward the outer edge. The corresponding autoradiographs (Figure 7F) indicated that the concentration of the radiolabeled antibody was much higher in the tumors than that in the normal liver, with a mean count ratio of approximately 10:1.

DISCUSSION

In this study, we investigated the distribution of ch14.18-ΔC_H2, an engineered immunoprotein labeled with ^{64}Cu via a series of sarcophagine and polyaza polycarboxylate BFCs. This study was prompted by our observation that the kidney concentration of ^{64}Cu-SarAr-ch14.18-ΔC_H2 was extremely high. The result is consistent with the report by Di Bartolo et al., who observed high kidney uptake (>200% ID/g) when using SarAr to label B72.3 F(ab′)$_2$.[23] These results led to the hypothesis that the high renal concentration was a consequence of the high positive charge associated with the Cu^{II}-SarAr moiety, and a series of sar

DOI: 10.1021/acs.bioconjchem.5b00049
Bioconjugate Chem. 2015, 26, 707−717

BFCs was prepared with different charges. The biodistribution of the ^{64}Cu-labeled RICs prepared using these BFCs showed a large range of uptake by the kidneys: from 47% ID/g for $^{64}Cu^{II}$-SarAr (net local change in charge, +4) to 28% ID/g for $^{64}Cu^{II}$-$(CH_3)(CO_2)$sar (net local charge increase, +1) to 6.6% ID/g for $^{64}Cu^{II}$-$(SO_3)(CO_2)$sar (net local charge increase, 0). Interestingly, $^{64}Cu^{II}$-$(NH_2)(CO_2)$sar-ch14.18-ΔC_H2 (net local charge increase, +2; renal uptake, 5.5% ID/g) does not seem to fit this pattern, as it has a higher apparent net charge and lower renal uptake. (To calculate net local change in charge, we considered the apical charge on the BFC at physiological pH (e.g., for SarAr = +1), the copper ion (+2), and the effect of reacting with the protein group (in the case of SarAr a loss of CO_2^-, so a net +1), giving a total of +4. We assumed that the secondary amines of the Sar cage would not be protonated following radiolabeling as the coordination of the metal ion would increase the acidity of the donor atoms.)

The reason that $^{64}Cu^{II}$-$(NH_2)(CO_2)$sar-ch14.18-ΔC_H2 does not fit this pattern can be understood when one considers the chemistry of the conjugation reaction between the BFC and the protein. In this study, the sar BFCs were conjugated to the protein using EDC, which reacts with carboxylates to form an *O*-acylisourea intermediate that can react with amines to form an amide bond. Thus, EDC will react with the carboxylic acid groups of $(CH_3)(CO_2H)$sar and $(SO_3H)(CO_2H)$sar and form amide bonds with amine residues (e.g., lysine) on the protein. Similarly, EDC will also react with carboxylic acid residues (e.g., glutamate) on the protein to form amide bonds with the aromatic or alkyl amine on SarAr. In the case of (NH_2)-(CO_2H)sar, both an alkyl amine and a carboxylic acid are present on the chelator, allowing for the formation of an amide bond either between the amine on the $(NH_2)(CO_2H)$sar and a carboxylic acid on the protein or the carboxylic acid on the $(NH_2)(CO_2H)$sar and an amine on the protein. If the carboxylic acid on the chelator reacts with an amine on the protein, then the result is that the amine on the chelator is exposed, presenting a positive charge to the environment. Conversely, if the amine on the chelator reacts with a carboxylate on the protein, then the net result is that the carboxylate is exposed, presenting a negative charge to the environment. Nakajima and Ikada[24] examined the mechanism of the EDC conjugation reaction and presented a strong argument in favor of the reaction between the primary amine of the $(NH_2)(CO_2H)$sar chelator and a carboxylate group on the protein. The results of the present study are in agreement with their conclusion in that the renal uptake of ^{64}Cu-(NH_2)-(CO_2H)sar-ch14.18-ΔC_H2 is similar to that of ^{64}Cu-(SO_3)-(CO_2)sar-ch14.18-ΔC_H2, which presents a negatively charged sulfonate to the environment, suggesting that the outer charge following conjugation with $(NH_2)(CO_2H)$sar is negative. The only previous use of $(NH_2)(CO_2H)$sar to radiolabel an antibody compared its performance in radiolabeling rituximab with seven other BFCs.[25] In that study, $(NH_2)(CO_2H)$sar was activated using EDC and then stabilized using sulfonated *N*-hydroxysuccinimide (sulfo-NHS), which was then reacted with the amine groups of the protein. In this case, EDC can only activate the carboxylate on the BFC because the protein is not yet present in the solution, and the resulting sulfo-NHS will react with an amine on the protein, leaving the amine of the $(NH_2)(CO_2H)$sar ligand exposed to the environment. Consistent with this premise, the kidney uptake of ^{64}Cu-$(NH_2)(CO_2H)$sar-rituximab was the highest of the BFCs investigated in that study.

The sarcophagine chelator SarAr was introduced as a BFC for labeling antibodies with ^{64}Cu as an alternative to the widely used DOTA, which lacks sufficient kinetic stability.[1] Accordingly, we compared the performance of the new sar chelators to three polyaza polycarboxylate BFCs (DOTA, NOTA, and BAT-6) that are also frequently used to label antibodies and other biomolecules with ^{64}Cu (Table 1). Among the three PAC chelators, the highest liver uptake was observed for DOTA (14% ID/g), whereas both BAT-6 (3.6% ID/g) and NOTA (4.0% ID/g) were significantly lower. Similarly, the concentration of ^{64}Cu-DOTA-ch14.18-ΔC_H2 in the blood and lung at 48 h p.i. was also higher than that of the BAT-6 and NOTA conjugates. Comparing the PAC BFCs to the new sar chelators, the renal concentration of the three PAC conjugates is generally lower than that of all of the sar-based chelators, although the differences are statistically significant only for SarAr and $(CH_3)(CO_2H)$sar. The liver concentrations of the BAT-6 and NOTA conjugates are lower than those of the other conjugates. These results suggest that the preferred BFC for labeling ch14.18-ΔC_H2 with ^{64}Cu is *p*-NCS-Bn-NOTA. This BFC contains three anionic carboxylate functional groups and thus forms mono anionic copper complexes, resulting in an RIC with lower retention in the kidneys compared to that of the positively charged conjugates that include cationic sarcophagine complexes.

The nature of the immunoprotein is also important in assessing these results. The ΔC_H2 format was generated for targeting GD2 because the (monovalent) Fab portion of the antibody ch14.18 failed to bind, suggesting that divalent binding was necessary for tumor targeting.[8] Moreover, ch14.18-ΔC_H2 has higher affinity for GD2 than does the whole antibody ch14.18 and has much faster clearance from the blood and other normal tissues.[8] The rapid clearance from the blood is due, at least in part, to the absence of the C_H2 domain, which contains three of the six amino acid residues required for interaction with the neonatal Fc receptor (FcRn) in the kidney, part of the recycling system that ensures antibodies in the blood are not continually excreted.[26] As the ΔC_H2 cannot be returned to the blood, it is excreted into the urine, facilitating its clearance from nontarget tissues.

This study is part of our continuing effort to develop an imaging agent for the detection and characterization of neuroblastoma metastases. Although several agents are currently available for imaging neuroblastoma, Reuland et al.[18] and Yeh et al.[21] observed that anti-GD2 antibodies may give an earlier indication of response to therapy than that with $^{123/131}$I-mIBG. A radiolabeled anti-GD2 antibody may also prove to be important in the evaluation of patients who are being considered for immunotherapy with nonradioactive hu14.18, the humanized version of the ch14.18 antibody.

To demonstrate the potential of ^{64}Cu-labeled ch14.18-ΔC_H2 for imaging neuroblastoma metastases, we carried out a preclinical imaging study in an orthotopic model of intrahepatic metastases using NOTA as the BFC. Focal uptake of ^{64}Cu-NOTA-ch14.18-ΔC_H2 was observed in the liver with minimal uptake in other areas (Figure 7). At necropsy, small lesions (<1 mm) were observed in the liver that were confirmed to be tumor by histological analysis and autoradiography. The apparently larger focal areas observed in the PET images of tumors detected by the PET camera are due to the physical limitations of the microPET system. The system resolution is approximately 1.4 mm, so partial volume averaging causes the lesions to appear to be much larger than they actually are and

DOI: 10.1021/acs.bioconjchem.5b00049
Bioconjugate Chem. 2015, 26, 707−717

to have lower RIC uptake. Interestingly, the images are similar throughout the two-day imaging study with the lesions being clearly seen as early as 4 h postinjection. This suggests that shorter half-life radionuclides, such as ^{68}Ga ($t_{1/2}$ = 68 min), could be used with NOTA-ch14.18-ΔC_H2, providing the same information while greatly reducing the time required between injection and imaging and the radiation dose to the patient.

In conclusion, these results support the hypothesis that the high renal uptake of ^{64}Cu-SarAr-ch14.18-ΔC_H2 was due to its high net positive charge, with Sar analogues having lower net positive charges showing lower uptake in the kidney. However, the PAC BFC conjugates all showed low tissue accumulation compared with that of the Sar-based chelators, with ^{64}Cu-NOTA-ch14.18-ΔC_H2 offering the greatest potential as an imaging agent for neuroblastoma. Future studies will focus on the use of the RIC to detect and characterize neuroblastoma metastases and monitor therapy response.

EXPERIMENTAL PROCEDURES

General. Chemicals and reagents were obtained from Sigma-Aldrich (St. Louis, MO) unless otherwise stated. Cell culture reagents were obtained from Mediatech (Herndon, VA) unless otherwise stated. Glassware was washed with 2 M nitric acid and rinsed with ultrapure water (>15 MΩ resistivity) (US Filter/Siemens Water Technologies, Warrendale, PA) before use. All solutions were prepared using ultrapure water. Metal contaminants in prepared solutions were decreased by passing the solutions through a Chelex-100 resin column (Bio-Rad Laboratories, Hercules, CA). Metal-naive pipet tips were purchased from Rainin Instrument (Oakland, CA). Copper-64 was purchased from Washington University−St. Louis (St. Louis, MO)[27] and was supplied in 0.04 M HCl. Radioactivity in the tissue samples was assayed with a Packard Cobra II automated gamma counter (Meriden, CT). Small-animal PET images were obtained using a Siemens Focus 120 camera (Siemens Medical Solutions USA, Malvern, PA) (BFC studies) or a Bruker Albira multimodality (PET/SPECT/CT) small-animal imaging system (Bruker Corporation, Woodbridge, CT) (metastatic model study). Computed Tomography (CT) images were obtained using a Siemens MicroCAT II scanner (Siemens Medical Solutions USA, Inc., Malvern, PA). The anti-GD2 engineered immunoprotein ch14.18-ΔC_H2[8] was kindly provided by Rupert Handgretinger, M.D. (Universität Tübingen, Germany). All animal procedures were carried out under a protocol approved by the Boston Children's Hospital Institutional Animal Care and Use Committee.

Bifunctional Chelators. The following BFCs were investigated in this study: 1-*N*-(4-aminobenzyl)-3,6,10,13,16,19-hexaazabicyclo[6.6.6]eicosane-1,8-diamine, SarAr; 5-((8-amino-3,6,10,13,16,19-hexaazabicyclo[6.6.6]-icosan-1-yl)amino)-5-oxopentoic acid, $(NH_2)(CO_2H)$sar; methyl 5-(8-amino-3,6,10,13,16,19-hexaaza-bicyclo[6.6.6]-icosan-1-ylamino-5-oxopentanoate, $(CH_3)(CO_2H)$sar; 5-oxo-5-(8-(2-sulfobenzamido)-3,6,10,13,16,19-hexaaza-bicyclo[6.6.6]icosan-1-ylamino)pentanoic acid, (SO_3H)-(CO_2H)sar; *S*-2-(4-aminobenzyl)-1,4,7,10-tetraazacyclododo-cane-1,4,7,10-tetraacetic acid, *p*-NH_2-Bn-DOTA; 6-[*p*-(bromoacetamido)benzyl]-1,4,8,11-tetraazacyclotetradecane-*N*,*N*′,*N*″,*N*‴-tetraacetic acid, BAT-6; and *S*-2-(4-isothiocyana-tobenzyl)-1,4,7-triazacyclononane-1,4,7-triacetic acid, *p*-NCS-Bn-NOTA. $(NH_2)(CO_2H)$sar and BAT-6 were generously donated by Matthew Harris, Ph.D. (Clarity Pharmaceuticals, Sydney, Australia) and Claude F. Meares, Ph.D. (UC Davis, Davis, CA), respectively. The compounds *p*-NH_2-Bn-DOTA and *p*-NCS-Bn-NOTA were purchased from Macrocyclics (Dallas, TX). SarAr[28] and $(CH_3)(CO_2H)$sar[29] were synthesized as described previously. All other reagents and solvents were obtained from standard commercial sources and were used as received. Nuclear magnetic resonance (NMR) spectra were acquired on a Varian FT-NMR 500 spectrometer and a Varian FT-NMR 400 spectrometer. ^{1}H NMR spectra were acquired at 500 or 400 MHz, and ^{13}C NMR spectra were acquired at 125.7 MHz. All NMR spectra were recorded at 25 °C. ^{1}H chemical shifts were referenced to the residual solvent peak, and ^{13}C chemical shifts were referenced to acetone in D_2O (δ = 30.89 and 215.94 ppm). ESIMS spectra were recorded on an Agilent 6510 ESI-TOF LC/MS mass spectrometer (Agilent, Palo Alto, CA). Microanalyses for C, H, and N were carried out by Chemical & Microanalytical Services (CMAS) Pty., Ltd. (Belmont, Victoria, Australia).

Synthesis of [Cu(NH$_3$)(CO$_2$CH$_3$)sar](CF$_3$SO$_3$)$_3$·0.5(C$_2$H$_6$O). To a solution of $(NH_2)(CO_2H)$sar[30] (0.20 g, 0.5 mmol) in distilled water (50 mL) was added copper acetate hydrate (0.10 g, 0.5 mmol), and the solution was stirred at room temperature for 2 h. The solution was applied to a column of Dowex 50WX2 cation exchange resin (H^+ form, 10 × 5 cm). The column was washed with H_2O (500 mL) and 1 M HCl (200 mL) and eluted with 3 M HCl (300 mL). The solution was taken to dryness under reduced pressure, leaving a purple residue. To the residue was added methanol (30 mL) followed by the dropwise addition of trifluoromethanesulfonic acid (~2 mL). The resulting blue solution was heated at reflux for 2 h. The solution was allowed to cool before the volatiles were removed under reduced pressure. The residue was cooled in an ice bath, and diethyl ether was added to precipitate a purple solid, which was collected by filtration and washed with copious amounts of diethyl ether. The purple solid was recrystallized from acetonitrile/diethyl ether followed by acetone/diethyl ether, collected by filtration, and dried to give $[Cu(NH_3)$-(CO_2CH_3)sar$](CF_3SO_3)_3$·$0.5(C_2H_6O)$ as a light blue powder (0.24 g, 24 mmol, 48%). Anal. Calcd for $C_{24}H_{46}CuF_9N_8O_{12.5}S_3$: C, 29.49; H, 4.74; N, 11.46. Found: C, 29.75; H, 5.15; N, 11.50. ESIMS: (+ve ion) calcd for $[Cu(NH_2)(CO_2CH_3)sar]^{2+}$ m/z 100%, 252.63; found, 252.63.

Synthesis of Cu(SO$_3$)(CO$_2$)sar·2.5(H$_2$O). To a solution of $[Cu(NH_3)(CO_2CH_3)sar](CF_3SO_3)_3$·$0.5(C_2H_6O)$ (0.09 g, 0.09 mmol) in anhydrous *N*,*N*-dimethylacetamide (2 mL) were added 2-sulfobenzoic anhydride (0.04 g, 0.2 mmol) in anhydrous *N*,*N*-dimethylacetamide (1 mL) and *N*,*N*-diisopropylethylamine (70 μL, 0.4 mmol) in anhydrous *N*,*N*-dimethylacetamide (1 mL). The solution was heated at 50 °C for 2 h. The reaction was monitored on a microcolumn of SP Sephadex C25 cation exchange resin (Na^+ form) eluted with 0.05 M sodium citrate. When a single, fast-moving band was detected, the reaction mixture was cooled, and water (50 mL) was added. The mixture was applied to a column of SP Sephadex C25 (Na^+ form, 6 × 3 cm), and after washing with water, the complex was eluted with 0.05 M sodium citrate. The major band was applied to a Dowex 50WX2 cation exchange column (H^+ form, 10 × 5 cm). After the column was washed with water (500 mL) and 1 M HCl (500 mL), the complex was eluted with 3 M HCl, and the eluent was evaporated to dryness under reduced pressure, leaving $[Cu(SO_3H)(CO_2H)sar]Cl_2$·$x$HCl as a purple residue (0.08 g). To the residue was added Dowex 1X8 anion exchange resin (acetate form). The resulting slurry was left standing with occasional swirling for 20 min

DOI: 10.1021/acs.bioconjchem.5b00049
Bioconjugate Chem. 2015, 26, 707−717

before being filtered through a sintered glass frit. Elution with water removed a blue solution that was concentrated to ~1 mL under reduced pressure. Methanol was slowly added until the solution was turbid. After standing at room temperature, fine blue needles were obtained that were collected by filtration. The crystals were washed with methanol and diethyl ether and then dried to give $Cu(SO_3)(CO_2)$sar·2.5(H_2O) (0.04 g, 0.05 mmol, 55%). Anal. Calcd for $C_{26}H_{47}CuN_8O_{9.5}S$: C, 43.41; H, 6.59; N, 15.58. Found: C, 43.26; H, 6.66; N, 15.53. ESIMS: (+ve ion) calcd for $[Cu(SO_3)(CO_2)sar + H^+]^+$ m/z 100%, 674.23; found, 674.23. ESIMS: (+ve ion) calcd for $[Cu(SO_3)(CO_2)sar + 2H^+]^{2+}$ m/z 100%, 337.62; found, 337.62. Crystals suitable for X-ray crystallography were grown by vapor diffusion of acetone into a solution of the complex in water.

Synthesis of $(SO_3H)(CO_2H)$sar·xHCl·xH_2O. The pH of an aqueous solution (20 mL) of $[Cu(SO_3H)(CO_2H)sar]Cl_2$·x$HCl$ (0.12 g, 0.16 mmol, based on $x = 0$) was increased to pH ~ 9 by addition of NaOH solution (0.2 M). The resulting blue solution was slowly added to a flask sparged with N_2 containing $NaBH_4$ (0.10 g) and Pd/C (0.50 g) in distilled water (20 mL), causing effervescence. The reaction mixture was stirred at room temperature overnight, and the resulting suspension was filtered through a 0.45 μm filter. The colorless filtrate was acidified with 1 M HCl (100 mL) and applied to a Dowex 50WX2 cation exchange column (H^+ form, 8 × 3 cm). After the column was washed with 1 M HCl solution (500 mL), the compound was eluted with 4 M HCl (175 mL). The eluate was evaporated to dryness under reduced pressure at 40 °C, leaving $(SO_3H)(CO_2H)$sar·xHCl·xH_2O as a colorless residue (0.09 g, 0.15 mmol, 94% approximately yield based on $x = 0$). ESIMS: (+ve ion) calcd for $[(SO_3H)(CO_2H)sar + H^+]^+$ m/z 100%, 613.31; found, 613.31. ^{1}H NMR (D_2O): δ 1.90 (m, 2H, CH_2), 2.38 (t, ^3J = 7.4 Hz, 2H, CH_2), 2.45 (t, ^3J = 7.2 Hz, 2H, CH_2), 3.1−3.9 (broad, 24H, cage CH_2), 7.48−7.52 (m, 1H, ArH), 7.64−7.69 (m, 2H, ArH), 7.91−7.94 (m, 1H, ArH). ^{13}C NMR (D_2O): δ 20.8, 33.4, 35.4 (glutarate CH_2), 46.9, 48.0, 51.4 (cage CH_2), 56.3, 57.4 (quat. C of cage cap), 127.7, 128.4, 131.4, 132.4, 133.4, 139.7 (ArC), 172.7, 177.8, 178.5, CO.

Crystallography. Intensity data for $Cu(SO_3)(CO_2)$sar·9H_2O were collected with an Oxford Diffraction SuperNova CCD diffractometer using Cu Kα radiation (graphite crystal monochromator λ = 1.54184 Å). The temperature during data collection was maintained at 130.0(1) K using an Oxford cooling device. Data were reduced and corrected for absorption.[31] The structures were solved by direct methods and difference Fourier synthesis.[32] Thermal ellipsoid plots were generated using ORTEP-3[33] integrated within the WINGX[34] suite of programs.

Conjugation of the BFCs to ch14.18-ΔC_H2. The ch14.18-ΔC_H2 antibody was buffer-exchanged and concentrated using centrifugal filter units (30 kDa MWCO; Centricon, Millipore, Billerica, MA). SarAr, $(NH_2)(CO_2H)$sar, $(CH_3)(CO_2H)$sar, $(SO_3H)(CO_2H)$sar, and p-NH_2-Bn-DOTA were conjugated to the antibody using the zero-length linker 1-ethyl-3-(3-(dimethylamino) propyl) carbodiimide hydrochloride (EDC; Pierce, Rockford, IL). The method for p-NH_2-Bn-DOTA is presented as an example. To 20 mg p-NH_2-Bn-DOTA in 50 μL Me_2SO (400 mg/mL) was added 3 volume equivalents of 0.1 M sodium acetate buffer (pH 5.0) to give a final BFC concentration of 100 mg/mL. The pH was brought to 5.0 by addition of 1 N NaOH. The chelator was added to the antibody at a molar ratio of 250:1 followed by sodium acetate buffer (to bring final protein concentration to 5 mg/mL) and then 500 mol equiv of EDC, prepared immediately before use in ultrapure water at a concentration of 50 mg/mL. After 30 min, unbound chelator was separated from the immunoconjugate by size-exclusion HPLC (BioSep SEC-S3000 column; Phenomenex, Torrance, CA) with an aqueous phase of 0.1 M sodium acetate, pH 5.0 (flow rate, 1 mL/min). The retention time of the immunoconjugate averaged 8.1 min, with the unbound chelator eluting at approximately 11.0 min. Purified immunoconjugate fractions were pooled, concentrated, and then stored in aliquots at −80 °C.

BAT-6 was conjugated to the immunoprotein as previously described.[35] Briefly, to 1 mg of protein (16.4 mg/mL) in 60.9 μL of tetramethylammonium phosphate buffer (pH 8.0) were added 0.133 μM BAT-6 in ultrapure water (9.25 μL) and freshly prepared 2-iminothiolane (2IT, 0.01 mg) in 50 mM triethanolamine hydrochloride (13.1 μL) at pH 8.7 such that final concentrations were as follows: Ab, 0.1 mM; BAT-6, 2 mM; and 2IT, 1 mM. The reaction was mixed by gentle pipetting, briefly centrifuged, and then placed in a 37 °C water bath for 30 min. Unbound chelator was removed by HPLC as before, and the immunoconjugate was concentrated into NH_4OAc buffer (0.1 M, pH 5.0) as previously described and stored in aliquots at −80 °C.

The conjugation of p-NCS-Bn-NOTA to ch14.18-ΔC_H2 was carried out as described by Vosjan et al.[36] Briefly, to 1 mg of ch14.18-ΔC_H2 (4 mg/mL) in sodium carbonate buffer (0.1 M, pH 9.1) was added 14.7 μL of p-NCS-Bn-NOTA (0.855 mg/mL) divided into three aliquots separated by 5 min (final molar ratio of Ab to BFC = 1:3). The reaction was mixed by gentle pipetting following each addition and then placed in a 37 °C water bath for 1 h. Unbound chelator was removed by HPLC as before, and the immunoconjugate was concentrated, buffer-exchanged into NaOAc buffer (0.1 M, pH 5.0) as before, and stored in aliquots at −80 °C.

Antigen Binding of Immunoconjugates. The bioactivity of the conjugated immunoproteins was assayed by enzyme-linked immunosorbent assay (ELISA). Lyophilized GD2 (Calbiochem, EMD Biosciences, Inc., La Jolla, CA) was dissolved in ethanol (20 μg/mL) and aliquoted into 96-well plates (100 μL per well). The plates were allowed to dry in a laminar flow hood overnight. Nonspecific protein binding was blocked for 1 h with 200 μL of phosphate buffered saline (PBS) containing 0.05% Tween 20, 1% bovine serum albumin (BSA) (w/v), and 1% normal goat serum (v/v). Following removal of the blocking solution, dilutions of the immunoproteins in the blocking solution were applied to the blocked wells and incubated for 2 h. The wells were then washed with PBS (200 μL × 3), and 100 μL horseradish peroxidase-conjugated goat anti-mouse polyclonal IgG (40 ng/mL; Jackson Laboratories, Bar Harbor, ME) diluted in PBS containing 0.05% Tween 20 and 1% BSA was applied to the wells. After 1 h, the wells were washed, and 100 μL of TMB peroxidase substrate solution (Kirkegaard & Perry Laboratories, Inc., Gaithersburg, MD) was applied to the wells, followed 20 min later by 100 μL of 1 M H_3PO_4. Absorbance (OD) was then read at 450 nm using an automated 96-well plate reader.

Isotope Dilution Assay. The ratio of available chelating molecules to protein molecules was measured as previously described[37] using the method reported by Meares et al.[38] except that ^{64}Cu was used instead of ^{57}Co. Briefly, a small amount of ^{64}Cu was added to a solution of known concentration of nonradioactive (cold) copper from a commercially available standard (Sigma-Aldrich, St. Louis,

DOI: 10.1021/acs.bioconjchem.5b00049
Bioconjugate Chem. 2015, 26, 707−717

MO) in acetate buffer (0.1 M, pH 5.0). An aliquot of immunoprotein conjugated with chelator was added and incubated for 1 h. The degree of labeling was then analyzed using thin-layer chromatography (ITLC SG, Biodex, Shirley, NY) developed with phosphate buffer (pH 8, 100 mM EDTA). Under these conditions, the labeled antibody remains at the baseline, and unbound ^{64}Cu travels at the solvent front. The number of available chelators was then calculated from the concentrations of immunoprotein, cold copper, and degree of incorporation.

Radiolabeling with ^{64}Cu. Three volume equivalents of sodium acetate buffer (0.1 M, pH 5.0) were added to 2 mCi ^{64}Cu in 5−10 μL HCl (0.04 N), and a solution of the antibody in acetate buffer (250 μg/75 μL) was then added to the ^{64}Cu solution. After 30 min incubation at 25 °C, the degree of radiolabeling was assessed by TLC using the same conditions as described above. If the TLC assay showed that the radiochemical purity was <95%, then the product was purified using centrifugal filter units and the postfiltration purity was confirmed by TLC. The radioimmunoconjugate was diluted with saline to give a final protein concentration of 0.5 mg/mL and sterile filtered (0.2 μm) before injection.

Biodistribution Studies. The ^{64}Cu-labeled antibody (50 μg antibody, 5.5 ± 1.5 MBq (149 ± 41 μCi)) was injected into the tail vein of athymic (nu/nu) female mice (The Jackson Laboratory, Bar Harbor, ME; 6−8 weeks of age and 20−25 g in weight). The mice were then anesthetized using isoflurane (1−4% in a flow of oxygen), and PET data were collected for 30 min at 24 and 48 h postinjection (p.i.). At 48 h p.i., CT images were obtained. After CT imaging, the mice were euthanized by CO_2 inhalation, and an *ex vivo* biodistribution analysis was performed. Tissues were collected and weighed, and the radioactivity was assayed. PET and CT images were registered manually using AMIDE software.[39] Data from volumes of interest (VOIs) were used to calculate the biodistribution in selected tissues for the small animal PET imaging studies.

Statistical Analysis. Statistical analysis was carried out using SPSS, ver. 19.0, for Windows. The 48 h *ex vivo* biodistribution data were analyzed by ANOVA with posthoc analysis using the Bonferroni correction. Differences were considered to be significant at the 5% level ($p < 0.05$).

Metastatic Model of Neuroblastoma. An imaging study was carried out to evaluate the ability of ^{64}Cu-labeled ch14.18-ΔC_H2 to localize to neuroblastoma liver metastases *in vivo*. IMR32 NB cells were purchased from the American Type Culture Collection (Manassas, VA) and grown in RPMI 1640 supplemented with antibiotics (100 U/mL penicillin and 100 μg/mL streptomycin), L-glutamine (2 mM), and 10% FCS (Atlantic Biologicals, Miami, FL) as a semicontinuous adhesion culture, with passaging by trypsinization every 3 to 4 days. Cells were used after 2 weeks of initiation of culture and were grown *in vitro* for no longer than 12 weeks. For tumor implantation, cells were trypsinized (0.05% trypsin, 0.53 mM EDTA in HBSS), pelleted by centrifugation, resuspended in medium, counted using a hemocytometer, recentrifuged, and resuspended in PBS at a concentration of 20 × 10^6 cells/mL. Athymic (nu/nu) female mice (The Jackson Laboratory, Bar Harbor, ME; 6−8 weeks of age and 20−25 g in weight) were anesthetized (1−4% isoflurane in oxygen), the spleen was exteriorized through an incision on the left side, and 1 × 10^6 cells in 50 μL were injected. Two minutes after injection of the tumor cells, the splenic vessels were tied off, and the spleen was removed. The inner wound was sutured, and the outer wound was closed using metal clips, which were removed approximately 9 days postsurgery. Meloxicam (5 mg/kg subcutaneous) was administered perioperatively for analgesia.

Three weeks postsurgery the mice were injected with ^{64}Cu-NOTA-ch14.18-ΔC_H2 (50 μg protein, mean of 75.7 μCi (range 55−90 μCi)) and were imaged at 1, 4, 24, and 48 h postinjection. After the final imaging session, the mice were euthanized by CO_2 inhalation, and samples of the liver were taken for histological analysis. Tissue was frozen in isopentane cooled in a slurry of isopropanol and frozen carbon dioxide and then stored at −80 °C. Tissues were sectioned (10 μm thickness) using a cryotome, air-dried, fixed in methanol, and then exposed to phosphor storage screens. The screens were scanned using a Fujifilm BAS-5000, and the resulting digital images of radionuclide distribution within the tissue were compared with the sections following hematoxylin and eosin (H&E) staining to demonstrate general morphology.

■ ASSOCIATED CONTENT

Ⓢ Supporting Information

Table S1: Crystallographic data for $Cu(SO_3)(CO_2)$sar. This material is available free of charge via the Internet at http://pubs.acs.org.

■ AUTHOR INFORMATION

Corresponding Author

*Tel.: 617-919-2106. Fax: 617-730-0619. E-mail: jason.dearling@childrens.harvard.edu.

Notes

The authors declare no competing financial interest.

■ ACKNOWLEDGMENTS

The authors express their gratitude to Erin Snay, Patricia Dunning, and Kathryn G. Commons, Ph.D., for technical assistance. The ch14.18-ΔC_H2 antibody was provided by Rupert Handgretinger, M.D., Universität Tübingen (Germany); the original protein and production cell line were developed and made available for use by Stephen Gillies, Ph.D., Provenance Biopharmaceuticals (Billerica, MA). This work was supported by National Institutes of Health grant 5K08CA093554 (to S.D.V.), by the Comunidad de Madrid (through the Madrid-MIT M+Visión Fellowship, to J.L.J.D.), the Children's Hospital Radiology Foundation, the Australian Research Council (to P.S.D.), and a Victoria Fellowship from the Victorian Government (to B.M.P.). Copper-64 was produced at Washington University School of Medicine (St. Louis, MO, USA) under the support of National Cancer Institute grant R24CA86307.

■ ABBREVIATIONS

BFC, bifunctional chelator; Sar, sarcophagine; PAC, polyaza polycarboxylate chelator; RIC, radioimmunoconjugate

■ REFERENCES

(1) Maheshwari, V., Dearling, J. L. J., Treves, S. T., and Packard, A. B. (2012) Measurement of the rate of copper(II) exchange for ^{64}Cu complexes of bifunctional chelators. *Inorg. Chim. Acta 393*, 318−323.

(2) Smith, S. V. (2004) Molecular imaging with copper-64. *J. Inorg. Biochem. 98*, 1874−901.

(3) Dearling, J. L., and Pedley, R. B. (2007) Technological advances in radioimmunotherapy. *Clin. Oncol. 19*, 457−469.

DOI: 10.1021/acs.bioconjchem.5b00049
Bioconjugate Chem. 2015, 26, 707−717

(4) Yokota, T., Milenic, D. E., Whitlow, M., and Schlom, J. (1992) Rapid tumor penetration of a single-chain Fv and comparison with other immunoglobulin forms. *Cancer Res. 52*, 3402−3408.
(5) Gillies, S. D., and Wesolowski, J. S. (1990) Antigen binding and biological activities of engineered mutant chimeric antibodies with human tumor specificities. *Hum. Antibodies Hybridomas 1*, 47−54.
(6) Slavin-Chiorini, D. C., Kashmiri, S. V., Schlom, J., Calvo, B., Shu, L. M., Schott, M. E., Milenic, D. E., Snoy, P., Carrasquillo, J., Anderson, K., et al. (1995) Biological properties of chimeric domain-deleted anticarcinoma immunoglobulins. *Cancer Res. 55*, 5957s−5967s.
(7) Chinn, P. C., Morena, R. A., Santoro, D. A., Kazules, T., Kashmiri, S. V., Schlom, J., Hanna, N., and Braslawsky, G. (2006) Pharmacokinetics and tumor localization of ^{111}In-labeled HuCC49-DeltaC_H2 in BALB/c mice and athymic murine colon carcinoma xenograft. *Cancer Biother. Radiopharm. 21*, 106−116.
(8) Mueller, B. M., Reisfeld, R. A., and Gillies, S. D. (1990) Serum half-life and tumor localization of a chimeric antibody deleted of the C_H2 domain and directed against the disialoganglioside GD2. *Proc. Natl. Acad. Sci. U.S.A. 87*, 5702−5705.
(9) Kushner, B. H. (2004) Neuroblastoma: a disease requiring a multitude of imaging studies. *J. Nucl. Med. 45*, 1172−1188.
(10) Howman-Giles, R., Shaw, P. J., Uren, R. F., and Chung, D. K. (2007) Neuroblastoma and other neuroendocrine tumors. *Semin. Nucl. Med. 37*, 286−302.
(11) Hero, B., Hunneman, D. H., Gahr, M., and Berthold, F. (2001) Evaluation of catecholamine metabolites, mIBG scan, and bone marrow cytology as response markers in stage 4 neuroblastoma. *Med. Pediatr. Oncol. 36*, 220−223.
(12) Matthay, K. K., Edeline, V., Lumbroso, J., Tanguy, M. L., Asselain, B., Zucker, J. M., Valteau-Couanet, D., Hartmann, O., and Michon, J. (2003) Correlation of early metastatic response by ^{123}I-metaiodobenzylguanidine scintigraphy with overall response and event-free survival in stage IV neuroblastoma. *J. Clin. Oncol. 21*, 2486−2491.
(13) Schulz, G., Cheresh, D. A., Varki, N. M., Yu, A., Staffileno, L. K., and Reisfeld, R. A. (1984) Detection of ganglioside GD2 in tumor tissues and sera of neuroblastoma patients. *Cancer Res. 44*, 5914−5920.
(14) Wu, Z. L., Schwartz, E., Seeger, R., and Ladisch, S. (1986) Expression of GD2 ganglioside by untreated primary human neuroblastomas. *Cancer Res. 46*, 440−443.
(15) Lode, H. N., Handgretinger, R., Schuermann, U., Seitz, G., Klingebiel, T., Niethammer, D., and Beck, J. (1997) Detection of neuroblastoma cells in CD34+ selected peripheral stem cells using a combination of tyrosine hydroxylase nested RT-PCR and anti-ganglioside GD2 immunocytochemistry. *Eur. J. Cancer 33*, 2024−2030.
(16) Cheung, I. Y., Sahota, A., and Cheung, N. K. (2004) Measuring circulating neuroblastoma cells by quantitative reverse transcriptase-polymerase chain reaction analysis. *Cancer 101*, 2303−2308.
(17) Fonti, R., Cheung, N. K., Bridger, G. J., Guo, H. F., Abrams, M. J., and Larson, S. M. (1999) 99mTc-monoclonal antibody radiolabeled via hydrazino nicotinamide derivative for imaging disialoganglioside GD2-positive tumors. *Nucl. Med. Biol. 26*, 681−686.
(18) Reuland, P., Geiger, L., Thelen, M. H., Handgretinger, R., Haase, B., Muller-Schauenburg, W., Niethammer, D., and Bares, R. (2001) Follow-up in neuroblastoma: comparison of metaiodobenzylguanidine and a chimeric anti-GD2 antibody for detection of tumor relapse and therapy response. *J. Pediatr. Hematol. Oncol. 23*, 437−442.
(19) Voss, S. D., Smith, S. V., DiBartolo, N., McIntosh, L. J., Cyr, E. M., Bonab, A. A., Dearling, J. L., Carter, E. A., Fischman, A. J., Treves, S. T., et al. (2007) Positron emission tomography (PET) imaging of neuroblastoma and melanoma with ^{64}Cu-SarAr immunoconjugates. *Proc. Natl. Acad. Sci. U.S.A. 104*, 17489−17493.
(20) Yu, A. L., Gilman, A. L., Ozkaynak, M. F., London, W. B., Kreissman, S. G., Chen, H. X., Smith, M., Anderson, B., Villablanca, J. G., Matthay, K. K., et al. (2010) Anti-GD2 antibody with GM-CSF, interleukin-2, and isotretinoin for neuroblastoma. *N. Engl. J. Med. 363*, 1324−1334.
(21) Yeh, S. D., Larson, S. M., Burch, L., Kushner, B. H., Laquaglia, M., Finn, R., and Cheung, N. K. (1991) Radioimmunodetection of neuroblastoma with iodine-131−3F8: correlation with biopsy, iodine-131−metaiodobenzylguanidine and standard diagnostic modalities. *J. Nucl. Med. 32*, 769−776.
(22) Dearling, J. L., Voss, S. D., Dunning, P., Snay, E., Fahey, F., Smith, S. V., Huston, J. S., Meares, C. F., Treves, S. T., and Packard, A. B. (2011) Imaging cancer using PET—the effect of the bifunctional chelator on the biodistribution of a ^{64}Cu-labeled antibody. *Nucl. Med. Biol. 38*, 29−38.
(23) Di Bartolo, N., Sargeson, A. M., and Smith, S. V. (2006) New ^{64}Cu PET imaging agents for personalised medicine and drug development using the hexa-aza cage, SarAr. *Org. Biomol. Chem. 4*, 3350−3357.
(24) Nakajima, N., and Ikada, Y. (1995) Mechanism of amide formation by carbodiimide for bioconjugation in aqueous media. *Bioconjugate Chem. 6*, 123−130.
(25) Cooper, M. S., Ma, M. T., Sunassee, K., Shaw, K. P., Williams, J. D., Paul, R. L., Donnelly, P. S., and Blower, P. J. (2012) Comparison of ^{64}Cu-complexing bifunctional chelators for radioimmunoconjugation: labeling efficiency, specific activity, and in vitro/in vivo stability. *Bioconjugate Chem. 23*, 1029−1039.
(26) Kenanova, V., Olafsen, T., Crow, D. M., Sundaresan, G., Subbarayan, M., Carter, N. H., Ikle, D. N., Yazaki, P. J., Chatziioannou, A. F., Gambhir, S. S., Williams, L. E., Shively, J. E., Colcher, D., Raubitschek, A. A., and Wu, A. M. (2005) Tailoring the pharmacokinetics and positron emission tomography imaging properties of anti-carcinoembryonic antigen single-chain Fv-Fc antibody fragments. *Cancer Res. 65*, 622−631.
(27) Kume, M., Carey, P. C., Gaehle, G., Madrid, E., Voller, T., Margenau, W., Welch, M. J., and Lapi, S. E. (2012) A semi-automated system for the routine production of copper-64. *Appl. Radiat. Isot. 70*, 1803−1806.
(28) Di Bartolo, N. M., Sargeson, A. M., Donlevy, T. M., and Smith, S. V. (2001) Synthesis of a new cage ligand, SarAr, and its complexation with selected transition metal ions for use in radioimaging. *J. Chem. Soc., Dalton Trans.*, 2303−2309.
(29) Paterson, B. M., Roselt, P., Denoyer, D., Cullinane, C., Binns, D., Noonan, W., Jeffery, C. M., Price, R. I., White, J. M., Hicks, R. J., et al. (2014) PET imaging of tumours with a ^{64}Cu labeled macrobicyclic cage amine ligand tethered to Tyr^3-octreotate. *Dalton Trans. 43*, 1386−1396.
(30) Ma, M. T., Karas, J. A., White, J. M., Scanlon, D., and Donnelly, P. S. (2009) A new bifunctional chelator for copper radiopharmaceuticals: a cage amine ligand with a carboxylate functional group for conjugation to peptides. *Chem. Commun.*, 3237−3239.
(31) *CrysAlis CCD*, version 1.171.32.5 (2007) Oxford Diffraction Ltd., Abingdon, England.
(32) Sheldrick, G. M. (2008) A short history of SHELX. *Acta Crystallogr., Sect. A 64*, 112−122.
(33) Farrugia, L. (1997) ORTEP-3 for Windows—a version of ORTEP-III with a Graphical User Interface (GUI). *J. Appl. Crystallogr. 30*, 565.
(34) Farrugia, L. J. (1999) WinGX suite for small-molecule single-crystal crystallography. *J. Appl. Crystallogr. 32*, 837−838.
(35) McCall, M. J., Diril, H., and Meares, C. F. (1990) Simplified method for conjugating macrocyclic bifunctional chelating agents to antibodies via 2-iminothiolane. *Bioconjugate Chem. 1*, 222−226.
(36) Vosjan, M. J., Perk, L. R., Visser, G. W., Budde, M., Jurek, P., Kiefer, G. E., and van Dongen, G. A. (2010) Conjugation and radiolabeling of monoclonal antibodies with zirconium-89 for PET imaging using the bifunctional chelate *p*-isothiocyanatobenzyl-desferrioxamine. *Nat. Protoc. 5*, 739−743.
(37) Hamburger, A. W., and Salmon, S. E. (1977) Primary bioassay of human tumor stem cells. *Science 197*, 461−3.
(38) Meares, C. F., McCall, M. J., Reardan, D. T., Goodwin, D. A., Diamanti, C. I., and McTigue, M. (1984) Conjugation of antibodies with bifunctional chelating agents: isothiocyanate and bromoacetamide reagents, methods of analysis, and subsequent addition of metal ions. *Anal. Biochem. 142*, 68−78.

DOI: 10.1021/acs.bioconjchem.5b00049
Bioconjugate Chem. 2015, 26, 707−717

(39) Loening, A. M., and Gambhir, S. S. (2003) AMIDE: a free software tool for multimodality medical image analysis. *Mol. Imaging 2*, 131−137.

DOI: 10.1021/acs.bioconjchem.5b00049
Bioconjugate Chem. 2015, 26, 707−717